Thin Solid Films 518 (2010) 5104–5109

Contents lists available at ScienceDirect

Thin Solid Films

journal homepage: www.elsevier.com/locate/tsf

Carbide and nanocomposite thin films in the Ti–Pt–C system

Erik Lewin [a,*], Kristina Buchholt [b], Jun Lu [c], Lars Hultman [c], Anita Lloyd Spetz [b], Ulf Jansson [a]

[a] Department of Materials Chemistry, The Ångström Laboratory, Uppsala University, Box 538, SE-751 21 Uppsala, Sweden
[b] Division of Applied Physics ,Department of Physics, Chemistry and Biology, IFM, Linköping University, SE-581 31 Linköping, Sweden
[c] Thin Film Physics Division, Department of Physics, Chemistry and Biology, IFM, Linköping University, SE-581 31 Linköping, Sweden

ARTICLE INFO

Article history:
Received 15 October 2009
Received in revised form 28 February 2010
Accepted 2 March 2010
Available online 16 March 2010

Keywords:
Solid solution carbide
Nanocomposite
Sputtering
Gas sensor
Annealing
Transmission electron microscopy
X-ray photoelectron spectroscopy
X-ray diffraction

ABSTRACT

Thin films in the Ti–Pt–C system were deposited by non-reactive, DC-magnetron sputtering. Samples were characterised using X-ray photoelectron spectroscopy, X-ray diffraction, and transmission electron microscopy. A previously not reported metastable solid solution carbide, $(Ti_{1-x}Pt_x)C_y$ with a Pt/Ti ratio of up to 0.43 was observed. This solid solution phase was present both as single phase in polycrystalline samples, and together with amorphous carbon (a-C) in nanocomposite samples. Annealing of nanocomposite samples leads to the decomposition of the solid solution phase and the formation of a nc-TiC_x/a-C/nc-Pt nanocomposite. Test sensors for automotive gas exhausts manufactured from such a three-phase material suffer from complete oxidation of the coating at 400 °C with no observed sensor activity.

1. Introduction

Field effect sensors with Pt as catalytic gate material have been shown useful for combustion control applications in wood fired boilers [1], and for NH_3 detection in selective catalytic reduction (SCR) systems as well as for lambda cold start sensors [2]. In field effect devices, the sensor response depends on the interaction between the catalytic gate material and the gas molecules. By modifying the gate material it is possible to change the selectivity of the sensor. Thin metal films (e.g. Pt, Pd, Ag, Au, or Ir) are used as catalytically active sensing layers on field effect devices. These films however often suffer from serious reconstruction when they are exposed to corrosive gases and/or are operated at higher temperatures [3]. The use of nanostructured films as gate material has the potential to give sensors with increased sensitivity, and faster response and recovery times due to the large surface to mass ratio. Also, nanostructured films are expected to give the possibility to tune the gas sensing properties by varying the size of the nanoparticles [4], and furthermore, by "locking" the nanoparticles into a matrix a more stable sensing layer could be achieved. Structures with such embedded crystallites of Ag have been synthesised with nc-TiC_x/a-C and nc-TiC_x/a-SiC as base material [5,6]. Pt is, however, preferred over Ag as a catalytic agent due to its higher melting point, i.e. better thermal stability. Hence, the possibility of producing nanocomposite coatings with Pt and TiC_x/a-C is interesting to investigate [3,7–9].

There are, however, complicating factors for the direct deposition of such structures, which are related to the formation of carbides. Transition metals have different abilities to form carbides. Strong carbide formers are found in groups 3–6, which form thermodynamically stable carbides. Groups 8–10 are weak carbide formers. Metastable carbides are known for Fe, Co, Ni, and Pt [10,11]. No carbides are known for groups 11–12 (where Ag and Cu are found).

In experimental [12,13] and theoretical [14] studies it has been found that weak carbide forming transition metals (Me) can form solid solutions with a strong carbide former, e.g., Ti. These solid solution carbides are found to contain much more Me than thermodynamical equilibrium allows, and are hence supersaturated. The weak carbide former substitutes some of the Ti, forming $(Ti_{1-x}Me_x)C$. This has, e.g., been shown for the Ti–Fe–C, Ti–Ni–C, and Ti–Cu–C systems [15–17]. It has also been shown that these metastable solid solutions can decompose by forming a separate metal phase of the weak carbide former [15–18]. It should hence be possible to produce the desired nc-TiC_x/a-C/nc-Pt structure, either during codeposition of the elements, or by codeposition followed by post-deposition annealing of metastable $(Ti_{1-x}Pt_x)C$ thin film.

The aim of the present study is two-fold: to investigate the phase and microstructure evolution of sputtered Ti–Pt–C coatings as a function of composition, and to investigate the possible synthesis of nc-TiC/a-C/nc-Pt coatings and their possible use in gas sensors.

* Corresponding author.
E-mail address: erik.lewin@mkem.uu.se (E. Lewin).

0040-6090/$ – see front matter © 2010 Elsevier B.V. All rights reserved.
doi:10.1016/j.tsf.2010.03.017

2. Experimental details

2.1. Materials

Deposition was carried out in an ultra high vacuum chamber (base pressure 10^{-7} Pa) by non-reactive, unbalanced DC-magnetron sputtering from separate 2 in. elemental targets, supplied by Kurt J. Lesker Company Ltd. (Ti and C, purity specified as 99.995% and 99.999%, respectively) and Johnson Matthey (Pt, purity specified as 99.99%). The Ar-plasma was generated at a constant pressure of 0.4 Pa, with a flow rate of Ar into the chamber of 150 sccm. Sputter deposition rates of respective element were controlled by regulation of the magnetron currents. Through tuning of magnetron currents samples were deposited in two series with varying Pt-content, see Fig. 1. Sample thickness was kept constant at about 1000 Å for a first batch of coatings and 500 Å for later depositions used in annealing experiments. Substrates were placed about 15 cm below the magnetrons on a rotating substrate holder and depositions were carried at with unheated substrates. Si with either native oxide or a 1000 Å thick thermally produced oxide was used as substrate.

Annealing of the films was performed in a vacuum furnace (base pressure 10^{-5} Pa). Annealing was performed for 1 h at temperatures between 650 °C and 850 °C. Heating and cooling were performed rapidly by moving the furnace over and away from the silica tube of the vacuum system. Comparing with previous studies on the Ti–Fe–C and Ti–Ni–C systems [15–18], these temperatures should be sufficient for the metastable solid solution to decompose and crystallise the weak carbide forming metal.

2.2. Characterisation

The principal methods of film characterization were X-ray photoelectron spectroscopy (XPS) for compositional analysis, and X-ray diffraction (XRD) for structural analysis. XPS was carried out on a Physical Electronics Systems Quantum 2000 spectrometer using monochromatic Al Kα radiation. For all films, depth profiles were acquired to determine the sample composition. High-resolution XPS spectra for binding analysis were recorded after sputter etching to a depth of ~150 Å. All sputter etching was performed with Ar^+, using an ion energy of 200 eV to minimise potential sputter-damage [19]. Curve fittings were performed using Voight-functions with a 20% Gaussian contribution and a Shirley-type background. Due to the likely presence of some sputter-damage, only simple curve fittings with three contributions were performed, and conclusions limited accordingly. XRD measurements were carried out on a Philips X'pert diffractometer, performing grazing incidence (GI) scans with parallel beam geometry. All XRD measurements were performed using Cu Kα radiation. Transmission electron microscopy (TEM) was performed using a Tecnai G2 TF20UT FEG microscope operated at 200 kV with a point resolution of 1.9 Å. Cross-sectional samples were prepared by the traditional method of mechanical and ion thinning.

Finger electrode structures consisting of 50 Å Cr + 3000 Å Au, for resistivity measurements of the films, were deposited by thermal evaporation through a mask on top of the films. A computer-controlled gas mixing system was used for a flow of the test gases over the sensor surfaces at 100 ml/min. During the measurements the sensors were exposed to the following series of test gases: NO_2, C_3H_6, H_2, CO, and NH_3. Nitrogen with 20% O_2 was used as the carrier gas. Gas sensing measurements were performed while keeping the sensors at 400 °C using a temperature control setup.

3. Results and discussion

As can be seen from Fig. 1, all Pt-containing samples have a Pt-content exceeding the thermodynamical solubility of Pt in TiC_x. Results of XRD on the as-deposited coatings are shown in Fig. 2.

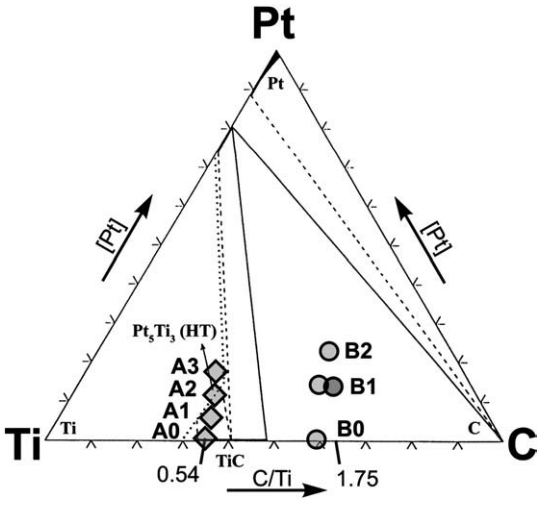

Fig. 1. Composition of the deposited coatings, marked in a phase diagram reproduced from Ref. [29]. Samples are denoted Ax and Bx in respective series. Diamond shapes are used for polycrystalline single-phase samples, and circles for nanocomposite samples. Sample B1 deposited twice, once at the same time as other samples, and also later for annealing experiments (darker marker).

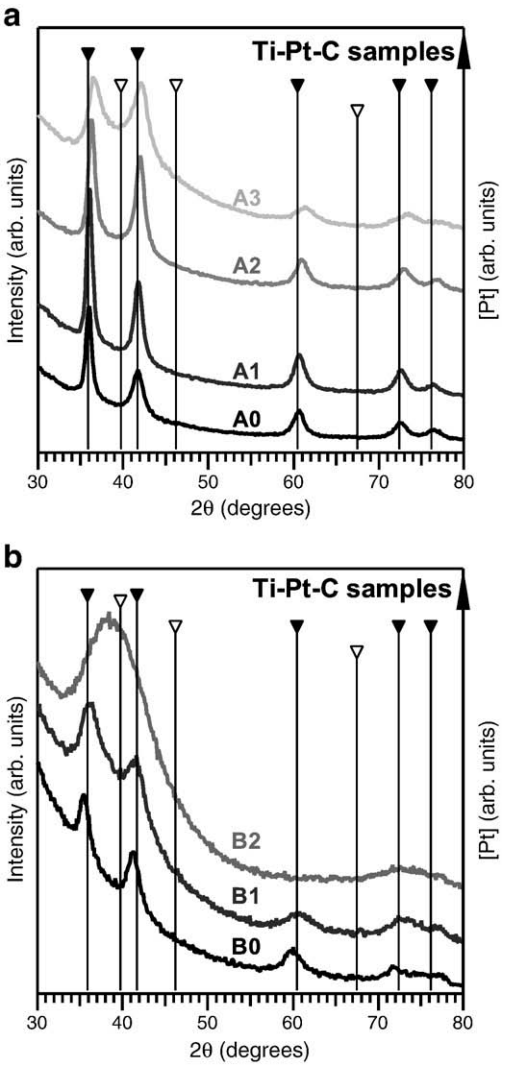

Fig. 2. GIXRD of the two sample series shown in Fig. 1. Pt-content increases upwards in both parts. Triangles mark reference positions for TiC (filled) and Pt (open) [30,31].

Generally only diffraction peaks matching TiC_x are observed. None of the intermetallic Ti–Pt phases match the observed diffraction pattern. A systematic shift of the peak positions to higher angles is also observed as the Pt-content increases. This gives a lattice parameter that (for the Ti-rich sample series) varies between 4.34 and 4.30 Å. A part of this shift can be attributed to a reduction in carbon content of the carbide, but this effect is too small (on the order of 0.015 Å) to account for the observed reduction [20]. Interestingly, it would be consistent with a substitutional solid solution of Pt (metallic radii: Pt = 1.39 Å and Ti = 1.45 Å) in the TiC_x phase, i.e. $(Ti_{1-x}Pt_x)C_y$. Lattice parameters and estimated grain sizes are presented in Table 1. There is also a consistent decrease in the TiC_x grain size as Pt-content increases. This observation is general for the case of solid solution carbides of strong and weak carbide formers [12,13,15,17].

A solid solution of Pt into the carbide is also supported by XPS results, primarily the Pt4f peak position of 71.6–71.7 eV, see Fig. 3. This is substantially different from the position found in metallic Pt, 71.0–71.2 eV and signifies a charge-transfer from Pt to a more electronegative element, i.e. C [21]. The C1s region of both sample series is shown in Fig. 4. As can be seen, the Ti-rich A-series (left) mainly show one type of carbon bonds, carbon bonded to Ti in the carbide phase at 281.7 eV [21–23]. For the carbon-rich B-series (right), there are two distinct types of bonding present: C–Ti from the carbide phase; and carbon bonded to carbon in an amorphous a-C phase at 284.2 eV [21,24,25]. Furthermore, a clear influence of the Pt-alloying can be observed in both series. In both series, the intensity around 282.6 eV increases as a result of Pt-alloying, this is where a contribution from C partly bonded to Pt and Ti would be expected, and is hence consistent with a solid solution carbide $(Ti_{1-x}Pt_x)C_y$. Overlapping with the C–Pt contribution is also a contribution, denoted C–Ti*, which originates from the interface nc-TiC|a-C [17,26]. Additionally, any sputter-damage is also expected to contribute to the intensity in this region [19]. A change in the relative amount of C–C and C–Me bonds is also observed in the nanocomposite B-series. The relative amount of a-C phase increases with Pt-content. This observation is consistent with observations from the Ti–Al–C, Ti–Fe–C, and Ti–Ni–C systems, where the solid solution of a weak carbide former in TiC_x was found to promote the formation of a-C phase during deposition [15–17,27]. The formed $(Ti_{1-x}Pt_x)C_y$ is not a thermodynamically stable compound and is likely to decompose upon annealing considering the position of Pt in the periodic table and the lack of PtC_x at normal conditions.

It can hence be concluded that the A-series essentially are single-phase carbides: $(Ti_{1-x}Pt_x)C_y$. The B-series are found to be nanocomposites: nc-$(Ti_{1-x}Pt_x)C_y$/a-C. The presence of Pt can, however, not be excluded from sample B2. It should also be noted that, despite the low Ar^+ energy used during sputter etching, the C1s spectra of the nanocomposite B-series bear resemblance to heavily sputter-damaged samples in the Ti–Ni–C system [19]. This is taken as a further indication that the $(Ti_{1-x}Pt_x)C_y$ is metastable.

High-resolution TEM was performed on samples A2 and B2 in order to investigate the possible presence of small amounts of crystalline Pt. Micrographs are shown in Figs. 5 and 6, respectively. Electron diffraction of the A2-sample shows that the film is polycrystalline with an average grain size of 10–20 nm. The cell parameter of the crystal structure of A2 is close to, but somewhat

Table 1
Lattice parameters (a) and grain sizes (t) determined from GIXRD. The latter estimated through Scherrer's equation [32]. Sample compositions defined in Fig. 1.

Sample	a (Å)	t (nm)	Sample	a (Å)	t (nm)
A0	4.34	7	B0	4.37	5
A1	4.34	7	B1	4.33	3
A2	4.32	6	B2	–	<2
A3	4.30	3			

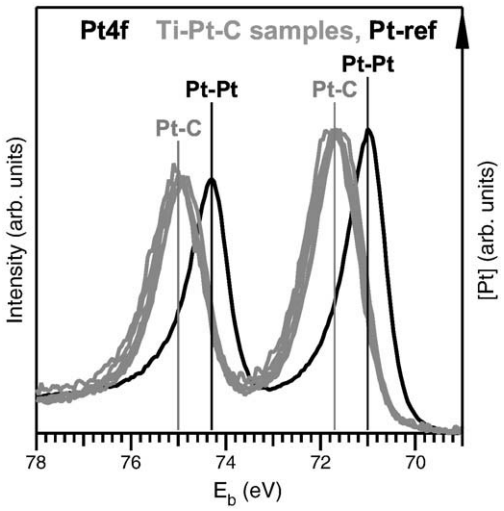

Fig. 3. High-resolution XPS spectra of the Pt4f region. Pt-reference sample with black line, samples A1–3 and B1–2 with grey lines. Spectra obtained after sputter etching, Ti–Pt–C samples sputtered to a depth of ~150 Å using 200 eV Ar^+ ions, and Pt reference sputtered with 4 keV Ar^+ ions.

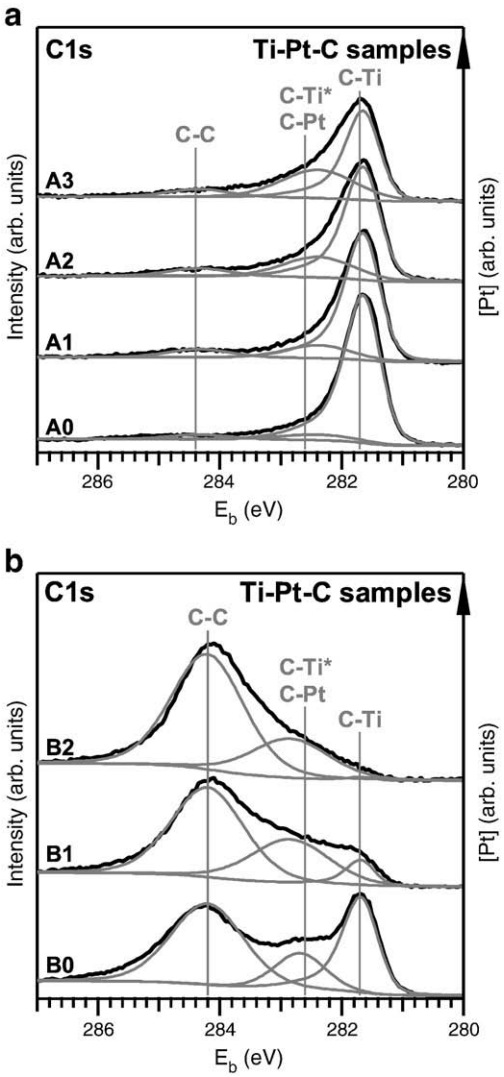

Fig. 4. High-resolution XPS spectra of the C1s region for all samples. Pt-content increases upwards. Spectra obtained after sputter etching to a depth of ~150 Å using 200 eV Ar^+ ions.

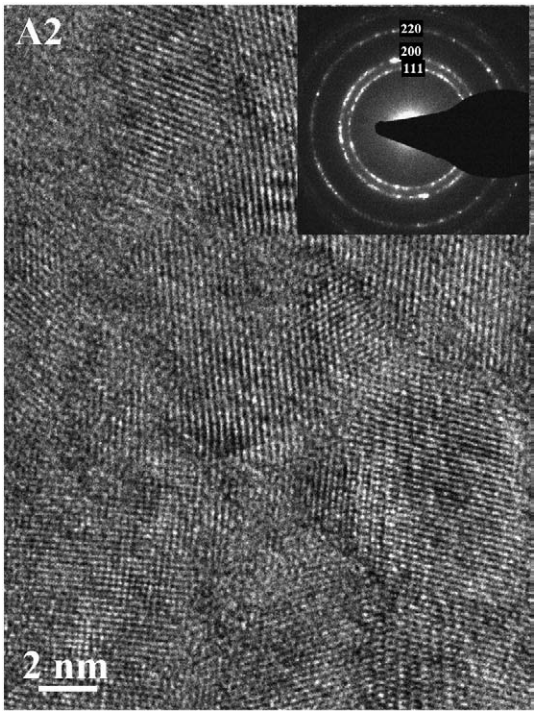

Fig. 5. HRTEM of the Ti-rich, Pt-alloyed sample A2, showing the polycrystalline morphology of the sample. Electron diffraction (inset) shows only diffraction matching the TiC-based carbide.

smaller than, the TiC_x structure. This confirms the single-phase structure of the A2-sample and that a solid solution carbide, $(Ti_{1-x}Pt_x)C_y$, has been formed. The B2-sample on the other hand shows an electron diffraction pattern typical of amorphous structures, and hence in agreement with the very wide 'peak' observed in XRD and suggesting that the coating is amorphous. However, the high-resolution images reveal that the sample also contains extremely small grains with an average size of 2–3 nm. The small grains are crystallites, or at least partly crystallized, most grains showed a periodicity that is close to that of metallic Pt, but a few grains showed a periodicity close to that of TiC_x. The sample thus consists of very small crystallites of Pt and $(Ti_{1-x}Pt_x)C_y$, as well as an amorphous a-C phase.

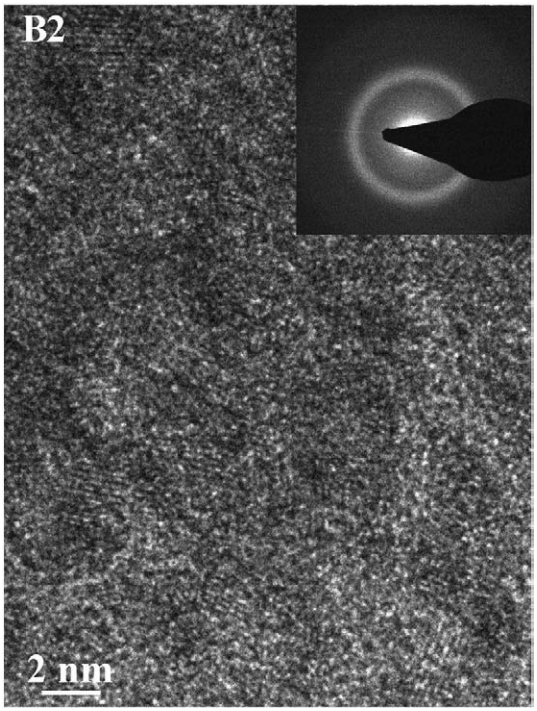

Fig. 6. HRTEM of the carbon-rich, Pt-alloyed sample B2. Despite the very broad electron diffraction (inset) lattice fringes can be observed in the sample. The periodicity of most of these fringes matches Pt.

Since a solid solution carbide phase was obtained in the as-deposited state, annealing experiments were conducted. This was both to study the decomposition of this phase and to obtain the microstructure with crystalline Pt embedded in a nc-TiC_x/a-C nanocomposite, which was sought after for gas sensor applications. The annealing experiments were performed on a second deposition of the B1 composition. The annealing resulted in an increased crystallinity of the carbide phase (from 650 °C) and the formation of a Pt-phase (from 750 °C), see Fig. 7.

To obtain additional information on the annealed samples, sputter depth profiles were acquired. These are shown in Fig. 8, where it can be seen that a redistribution of the elements takes place. Pt is found to migrate towards the substrate, as annealing temperature is increased. As can be seen from the sputter depth profiles the surface of the samples becomes enriched in Ti and O as annealing temperature increases, indicating a sample oxidation from the surface, despite the use of high vacuum conditions during annealing. Another interesting observation is that no increase of a-C phase could be noted. The only change in the C1s peak (not shown) upon annealing is the disappearance of the C–Pt bonds.

The observed migration of Pt towards the substrate is similar to what has been observed by Bijelovic et al. in the Ti–Fe–C system [18]. These different behaviours can be understood from the theoretical results of Hugosson et al., who show that the surface segregation energy of the group 11 metals in TiC is considerably lower than for the other transition metals [28]. This general segregation of Pt towards the substrate could hence make carbon- or carbide-based nanocomposites a poor choice for Pt-based sensors if annealing is required for the formation of Pt crystallites.

One B1-sample annealed at 850 °C, was tested as a gas sensor. In the test no response to any gases was observed. After the test, the coating had changed colour (from grey to bluish). To investigate the change of the coating, a sputter depth profile was obtained in the same way as above. The result is shown in Fig. 9. The coating was found to be totally oxidised. Almost all carbon had disappeared and the Ti2p peak showed that the vast majority of Ti is bonded to oxygen [21]. The probable cause of this complete oxidation is the catalytical

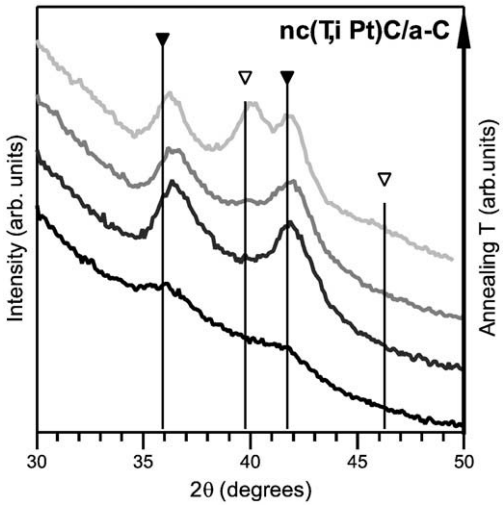

Fig. 7. GIXRD of the second B1-sample, as deposited (black, bottom) and annealed for 650, 750, and 850 °C (grey). Triangles mark reference positions for TiC (filled) and Pt (open) [30,31]. There is less intensity from the as-deposited sample than in Fig. 2 due to thinner coating and hence smaller diffraction volume.

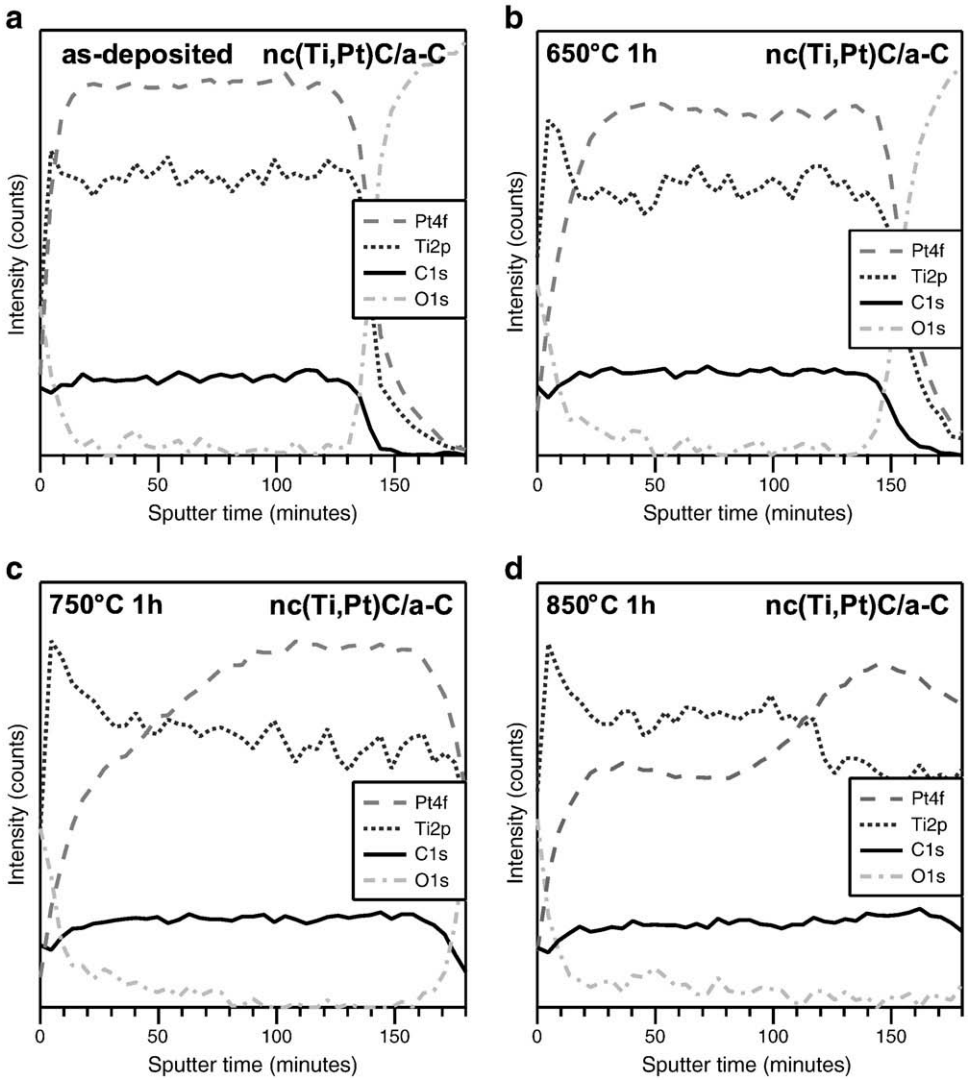

Fig. 8. XPS sputter depth profiles of annealed and as-deposited B1-samples. Sputter etching performed with 200 eV Ar^+ ions.

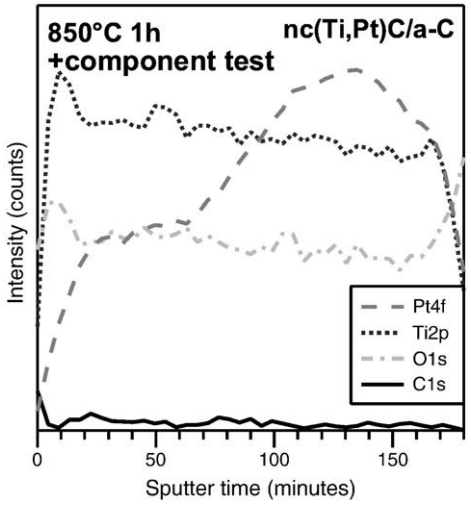

Fig. 9. Sputter depth profile of an annealed B1-sample after component tests with NO_2, C_3H_6, H_2, CO, and NH_3 in air at 400 °C. Sputter etching performed with 200 eV Ar^+ ions.

activity of Pt, producing oxygen radicals that rapidly react with both the carbide and the amorphous carbon. The Pt-profile from the annealing has been retained, despite substantial diffusion of other species.

4. Concluding remarks

We have synthesised single-phase carbides and nanocomposites in the Ti–Pt–C system using sputter deposition. In ternary samples a supersaturated solid solution carbide $(Ti_{1-x}Pt_x)C_y$ was formed. Annealing of nanocomposite samples containing this metastable carbide leads to its decomposition by formation of metallic Pt. It was found that the Pt segregated towards the substrate during annealing, which may reduce the catalytic efficiency of the Pt. Sensor tests with produced nc-TiC/a-C/nc-Pt coatings in oxidising environment at elevated temperatures lead to complete oxidation of the material.

Acknowledgements

The authors wish to acknowledge the financial support of the Swedish Research Council (VR), and Vinnova (Swedish Governmental Agency for Innovation Systems) through the VINN Excellence Centre FunMat.

References

[1] M. Andersson, L. Everbrand, A. Lloyd Spetz, IEEE Sens. Conference (2007) 962.
[2] H. Wingbrant, I. Lundström, A. Lloyd Spetz, Sens. Actuator, B 93 (2003) 286.
[3] H. Wingbrant, A. Lloyd Spetz, Sens. Lett. 1 (2003) 37.
[4] A. Salomonsson, S. Roy, C. Aulin, J. Cerdà, P.-O. Käll, L. Ojamäe, M. Strand, M. Sanati, A. Lloyd Spetz, Sens. Actuators, B 107 (2005) 831.
[5] J.L. Endrino, J.J. Nainaparampil, J.E. Krzanowski, Surf. Coat. Technol. 157 (2002) 95.
[6] P. Eklund, T. Joelsson, H. Ljungcrantz, O. Wilhelmsson, Z. Czigány, H. Högberg, L. Hultman, Surf. Coat. Technol. 201 (2007) 6465.
[7] H. Wingbrant, M. Lundén, A. Lloyd Spetz, Sens. Lett. 3 (2005) 225.
[8] H. Wingbrant, M. Persson, A.E. Abom, M. Eriksson, B. Andersson, S. Simko, D.J. Kubinski, J.H. Visser, A.L. Spetz, IEEE Sens. J. 6 (2006) 887.
[9] I. Lundström, H. Sundgren, F. Winquist, M. Eriksson, C. Krantz-Rülcker, A. Lloyd Spetz, Sens. Actuator, B 121 (2007) 247.
[10] P. Ettmayer, W. Lengauer, in: R.B. King (Ed.), Encyclopedia of Inorganic Chemistry, vol. 2, John Wiley & Sons Ltd, Chichester, 1994, p. 526.
[11] S. Ono, T. Kikegawa, Y. Ohishi, Solid State Commun. 133 (2005) 55.
[12] B. Trinidade, M.T. Vieira, Mater. Sci. Eng. 352 (2003) 195.
[13] G. Tomé, B. Trinidade, M.T. Vieira, Vacuum 64 (2002) 205.
[14] [14] M. Råsander, Licentiate thesis: theoretical investigations of ternary titanium carbide, Uppsala University, 2008.
[15] O. Wilhelmsson, S. Bijelovic, M. Lindquist, B. André, U. Wiklund, P. Svedlindh, U. Jansson, Thin Solid Films 518 (2009) 2607.
[16] O. Wilhelmsson, http://urn.kb.se/resolve?urn=urn:nbn:se:uu:diva-826522007.
[17] E. Lewin, http://urn.kb.se/resolve?urn=urn:nbn:se:uu:diva-1094272009.
[18] S. Bijelovic, M. Råsander, O. Wilhelmsson, E. Lewin, B. Sanyal, U. Jansson, O. Eriksson, P. Svedlindh, Phys. Rev. B: Condens. Matter 81 (2009) 014405.
[19] E. Lewin, M. Gorgoi, F. Schäfers, S. Svensson, U. Jansson, Surf. Coat. Technol. 204 (2009) 455.
[20] J.L. Murray, ASM International, Metal Parks, 1989.
[21] J. Moulder, W.F. Stickle, P.E. Sobol, K.D. Bomben, Physical Electronics, Inc., Eden Prairie, USA, 1995.
[22] L. Ramqvist, K. Hamrin, G. Johansson, A. Fahlman, C. Nordling, J. Phys. Chem. Solids 30 (1969) 1835.
[23] S.V. Didziulis, J.R. Lince, T.B. Stewart, E.A. Eklund, Inorg. Chem. 33 (1994) 1979.
[24] K. Hamrin, G. Johansson, U. Gelius, C. Nordling, K. Siegbahn, Phys. Scr. 1 (1970) 277.
[25] P.K. Chu, L.H. Li, Mater. Chem. Phys. 96 (2006) 253.
[26] E. Lewin, P.O.Å. Persson, M. Lattemann, M. Stüber, M. Gorgoi, A. Sandell, C. Ziebert, F. Schäfers, W. Braun, J. Halbritter, S. Ulrich, W. Eberhardt, L. Hultman, H. Siegbahn, S. Svensson, U. Jansson, Surf. Coat. Technol. 208 (2008) 3563.
[27] O. Wilhelmsson, M. Råsander, M. Carlsson, E. Lewin, B. Sanyal, U. Wiklund, O. Eriksson, U. Jansson, Adv. Funct. Mater. 17 (2007) 1611.
[28] H.W. Hugosson, O. Eriksson, U. Jansson, I.A. Abrikosov, Surf. Sci. 585 (2005) 101.
[29] P. Vilars, A. Prince, H. Okamoto, ASM International, London, 1995.
[30] M.C. Morris, H.F. McMurdie, E.H. Evans, B. Paretzkin, H. Parker, N.P. Pyrros, C.R. Hubbard, National Bureau of Standards (U.S.) Monograph 25 Section 18 (1981) 73.
[31] H.E. Swanson, E. Tatge, National Bureau of Standards (U.S.) Circular 539 vol. 1 (1953) 31.
[32] P. Scardi, M. Leoni, R. Delhez, J. Appl. Crystallogr. 37 (2004) 381.